APPLIED SCIENCES AND ENGINEERING

Conductance-stable liquid metal sheath-core microfibers for stretchy smart fabrics and self-powered sensing

Lijing Zheng[1], Miaomiao Zhu[2], Baohu Wu[3], Zhaoling Li[4], Shengtong Sun[1]*, Peiyi Wu[1]*

Highly conductive and stretchy fibers are crucial components for smart fabrics and wearable electronics. However, most of the existing fiber conductors are strain sensitive with deteriorated conductance upon stretching, and thus, a compromised strategy via introducing merely geometric distortion of conductive path is often used for stable conductance. Here, we report a coaxial wet-spinning process for continuously fabricating intrinsically stretchable, highly conductive yet conductance-stable, liquid metal sheath-core microfibers. The microfiber can be stretched up to 1170%, and upon fully activating the conductive path, a very high conductivity of 4.35×10^4 S/m and resistance change of only 4% at 200% strain are realized, arising from both stretch-induced channel opening and stretching out of tortuous serpentine conductive path of the percolating liquid metal network. Moreover, the microfibers can be easily woven into an everyday glove or fabric, acting as excellent joule heaters, electrothermochromic displays, and self-powered wearable sensors to monitor human activities.

INTRODUCTION

Flexible, stretchable, and lightweight conductors are the indispensable components of emerging wearable electronics (*1*), soft robotics (*2*), deformable supercapacitors/batteries (*3*), flexible displays (*4*), etc. Among them, stretchable fiber conductors that could be easily knitted into fabrics with high air permeability and unnoticeable size in wearing have attracted increasing interest (*5*, *6*). Researchers mainly focus on two categories of stretchable conductive fibers with extreme strain-dependent conducting properties for distinct purposes: fiber sensors with highly sensitive conductance changes and fiber electrodes/interconnects with stable conductance. Specifically, the recent developments in high-performance electronics have proposed very high demand for stretchable fiber electrodes/interconnects that could steadily transport electrical signals between active electronic components even under various and harsh mechanical deformations without notable conductance loss (*7*–*9*). However, in comparison with fiber strain sensors that have been extensively constructed by altering the conductive path via cracks (*10*, *11*), percolation (*12*), twisting (*13*), or even the intrinsic resistance response following Pouillet's law (in the case of constant conductivity, $R/R_0 = \lambda^2$; R and R_0 are the resistances before and after stretch, respectively, and λ is the deformation ratio) (*14*, *15*), it remains challenging to fabricate stretchable fiber conductors with stable yet consistently high conductance.

Most of stretchable fiber conductors are based on either a mixing or coating method to integrate an elastic fiber matrix with conductive fillers. Regardless of material selection, the electrical contact between conductive fillers determines the conductivity; during stretch, conductive fillers may separate from each other, leading to the deterioration of conductivity (*16*). As most conductive media are rigid with unchangeable conductivity, a generally adopted strategy to design strain-insensitive fiber conductors is to induce solely the geometric distortion of conductive path via a prestrain buckling process or simply shaping the fiber in wavy or helical structures (*7*, *17*–*24*). For example, Liu *et al.* (*7*) reported superelastic conducting sheath-core fibers with a hierarchically buckled sheath prepared by wrapping carbon nanotube sheets on prestretched rubber fiber cores, which enables a resistance change of less than 5% for a 1000% stretch. Recently, inspired by the peristaltic behavior of arthropods, coating worm-shaped buckled graphene microlayer on a polyurethane filament also leads to strain-insensitive resistance change of less than 0.1 up to 220% strain (*20*). Notwithstanding the success of these pioneered studies, the drawbacks of these strategies are also apparent: First, the nonstretchable conductive materials easily fragment and delaminate from the elastomeric polymers, leading to low conductivity and durability (*25*). Second, the complicated two- or more-step processes do not allow for the continuous fabrication of long strain-insensitive fiber conductors. Third, as most of the conductive layers are exposed outside, leakage of conductive materials and environmental influence on the fiber conductivity will become another tricky issue.

To overcome these limitations, we consider that embedding deformable conductive fillers with strain-enhanced conductivity into an elastic matrix may produce ultralong, intrinsically stretchable fiber conductors with both stable and high conductance. Liquid metal (LM) is a kind of low–melting point metal or alloy material with unique advantages of high electrical conductivity [eutectic gallium-indium (EGaIn): 3.4×10^6 S/m], room temperature fluidity, environmental stability, and biocompatibility (*26*, *27*). Although plenty of studies have attempted to encapsulate pure LM into elastomer hollow tubes or coat LM onto stretchable fibers to maintain high conductivity even at very high elongations (*28*–*35*), these conductive fibers still have ever-changing conductance (basically obeying Pouillet's law), and LM leakage often occurs. On the other hand, note that several recent studies have implied the unconventional positive piezoconductivity effect of LM-embedded elastomers arising from the stretch-induced elongation of LM particles

[1]State Key Laboratory for Modification of Chemical Fibers and Polymer Materials, College of Chemistry, Chemical Engineering and Biotechnology & Center for Advanced Low-dimension Materials, Donghua University, Shanghai 201620, China. [2]College of Materials Science and Engineering, Donghua University, Shanghai 201620, China. [3]Jülich Centre for Neutron Science (JCNS) at Heinz Maier-Leibnitz Zentrum (MLZ) Forschungszentrum Jülich, Lichtenbergstr. 1, 85748 Garching, Germany. [4]College of Textiles, Donghua University, Shanghai, 201620, China.
*Corresponding author. Email: shengtongsun@dhu.edu.cn (S.S.); wupeiyi@dhu.edu.cn (P.W.)

(piezoconductivity: the composite shows an increased conductivity under tensile strain while most conductive composites show an increased resistivity) (*16*, *36*–*38*). It is therefore believed that LM may represent one of the best candidate conductive fillers for fabricating conductance-stable, intrinsically stretchable fiber conductors.

With these concerns in mind, this work put forward a coaxial wet-spinning method to continuously prepare superelastic LM sheath-core microfibers with both high and ultrastable conductance. The sheath of the microfiber is composed of double-network fluoroelastomer with good elasticity, and the core is the composite of the same fluoroelastomer and percolated LM (EGaIn alloy) nanoparticles. The sheath-core structure and the dipole-dipole interactions between fluoroelastomer and LM make the embedded LM particles in the core conformally deform upon stretching, leading to both high stretchability and as-expected conductance stability without the concern of LM leakage. Compared with the previously reported strain-insensitive fiber conductors, the present LM sheath-core microfibers exhibit great advantages in large-scale fabrication and impressive mechanical and electrical performance (maximum strain, ~1170%; only 4% resistance change at 200% strain; high initial conductivity, ~4.35 × 10^4 S/m; relatively low modulus, ~2.16 MPa). Here, we further explored the promising applications of the resulting LM sheath-core microfibers in smart fabrics and self-powered sensing based on joule heating, electrothermochromism, and triboelectric properties.

RESULTS

Preparation of LM sheath-core microfibers

Figure 1A and fig. S1 show the illustrations of the coaxial wet-spinning process for preparing LM sheath-core microfibers. To improve the fiber quality by smoothly solidifying the spinning solution, we used a triaxial wet-spinning needle with the inner, middle, and outer diameters of 400, 1950, and 3000 μm, respectively, which was further immersed into deionized (DI) water as the coagulating bath. Correspondingly, the three spinning solutions are PVDF-HFP-TFE [poly(vinylidene fluoride-hexafluoropropylene-tetrafluoroethylene)]/EGaIn particle/MEK (methyl ethyl ketone) in the inner channel, PVDF-HFP-TFE/PEGDA [poly(ethylene glycol) diacrylate]/Irgacure 184/MEK in the middle channel, and DI water in the outer channel, respectively. Among them, the fluoroelastomer, PVDF-HFP-TFE, with a molar ratio of VDF [48 mole percent (mol %)], HFP

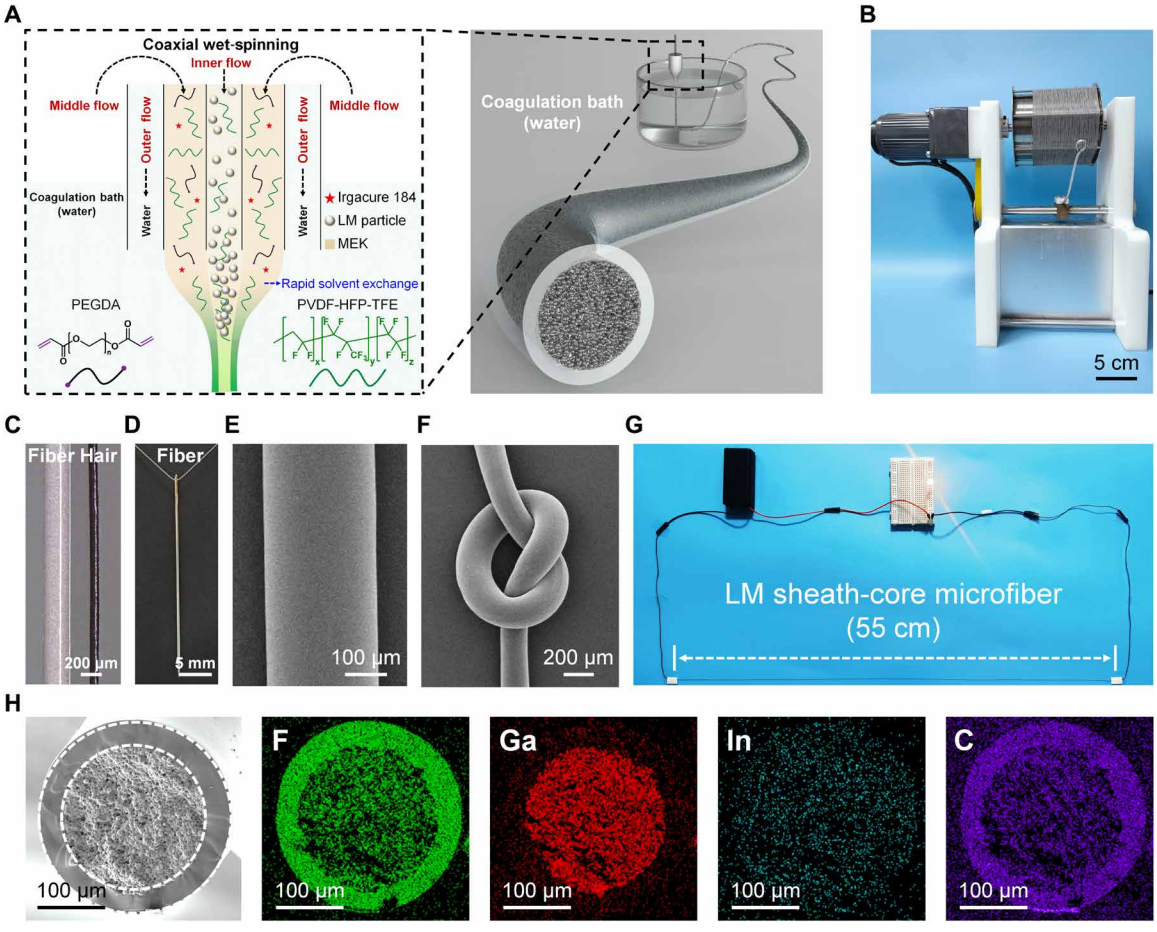

Fig. 1. Preparation of LM sheath-core microfibers. (**A**) Schematic setup and the main components for the coaxial wet-spinning process for producing LM sheath-core microfibers. (**B**) A single as-spun fiber with the length of 380 m was collected on a continuously winding collector. (**C**) Microscopic images of LM sheath-core microfiber and human hair. (**D**) Photo of the microfiber threaded into a needle. (**E**) SEM image of the external surface of the microfiber. (**F**) SEM image of a knotted microfiber. (**G**) An LED can be lit up through a 55-cm-long activated LM sheath-core microfiber at a voltage of 3 V. (**H**) The cross-sectional SEM and corresponding elemental mapping images of the microfiber. Photo credit: Lijing Zheng, Donghua University.

(19 mol %), and TFE (33 mol %) [see nuclear magnetic resonance characterizations and calculation details in figs. S2 and S3 and the Supplementary Materials], was chosen owing to its good stretchability and electrical insulativity when solidified (*39*). The concentrations of PVDF-HFP-TFE in the middle and inner spinning solutions were optimized to be 360 and 300 mg/ml, respectively, and its content in the final solidified core was adjusted from 3 to 11 weight % (wt %) as a controlling variable. As illustrated in Fig. 1A, when the three solutions contact each other at the spinning head, MEK is quickly exchanged with water in the outer flow, leading to the curing of both sheath and core components. We highlight here the importance of sheath-core design for fabricating LM microfibers; without the protection of the fluoroelastomer sheath, LM leakage may easily occur (fig. S4), which has increasingly become an issue that has to be faced in the practical uses of LM composite materials (*40*). Furthermore, to improve the toughness and elastic recovery of the LM sheath-core fiber (*41*), we introduced a second covalent network in the sheath by post–ultraviolet-polymerizing the added difunctional monomers, PEGDA (M_n: 250 g/mol), in the middle spinning solution.

With this method, the LM sheath-core microfibers can be continuously wet-spun into ideally unlimited length (see an example of 380-m-long fiber in Fig. 1B). After fully drying, the microfiber is rather smooth with a diameter of ~270 μm, a little larger than human hair (Fig. 1C), and can be easily threaded into a needle (Fig. 1D). The scanning electron microscopy (SEM) image further shows the uniform and regular surface of the fiber (Fig. 1E) and its flexibility (Fig. 1F). Good electrical conductivity of the fibers was demonstrated by lighting a light-emitting diode (LED) with a 55-cm-long fiber at a small voltage of 3 V (Fig. 1G). As shown in Fig. 1H, the cross-sectional SEM image of the fiber shows clearly the sheath-core structure with a smooth fluoroelastomer sheath and rough LM-fluoroelastomer composite core. Corresponding elemental mapping images identify the distributions of Ga and In elements only in the core and those of F and C elements concentrated in the sheath yet sparse in the core, in good accordance with the spinning recipe. An enlarged view (fig. S5) of the composite core indicates the homogeneous distribution of LM particles in the fluoroelastomer matrix, and the embedded LM particles have sizes ranging from 0.8 to 7 μm (mean size, ~3.6 μm; see the statistical analysis in fig. S6). Moreover, the cross-sectional Raman imaging of the microfiber again implies the obvious sheath-core boundary scanned at two characteristic vibrational bands for fluoroelastomer and LM, respectively (fig. S7).

Mechanical properties and strain-insensitive conductance

The LM sheath-core microfibers are highly elastic with good stretchability and cyclability. Taking the microfiber with 7 wt % fluoroelastomer in the core for example (unless otherwise stated, all the mentioned microfibers in this paper are based on this concentration), the fiber can be stretched up to 11.7 times longer than the original length with the Young's modulus of 2.16 MPa; the loading-unloading curves at increasing strains (100 to 1000%) also coincide well with the single tensile curve to break (Fig. 2A). It is noted that because of the fluidity of LM, the modulus of the whole sheath-core microfiber is much lower than pure fluoroelastomer fiber (Young's modulus, ~3.2 MPa; fig. S8), suggesting its good compliance with fabrics and human skin. The good elastic recovery of the microfiber is supported by the cycling tensile tests at a fixed strain of 100% for 100 cycles (Fig. 2B), which shows almost overlapped cycling curves after the first cycle (irreversible structures were disrupted in the first cycle). Replotting the tensile curve in the Mooney-Rivlin representation (*42*) shows clearly three sequential stages, and a long plastic deformation range from 32 to 670% strain is attributed from both the fluoroelastomer and the plastically deformable LM particles (fig. S9).

To make the as-spun LM sheath-core microfiber electrically conductive, activation is usually necessary to rupture the initially resistive oxidation layer on LM particles and make them coalesce into a percolating network. In this work, we used a sequential "freezing-plus-stretching" strategy to fully sinter the LM particles for conductivity activation. Since LM has abnormal volume expansion behavior, which expands rather than shrinks at low temperatures (*43*, *44*), liquid nitrogen freezing-induced phase and stiffness change can help LM particles pierce through the oxide and elastomer coating layers to contact each other, leading to the partial activation of the conductive path (fig. S10). As shown in Fig. 2C, subsequent mechanical stretching to 200% drastically reduced the resistance to a much lower level corresponding to a considerably high conductivity of ~4.35×10^4 S/m, and then repeated stretching and recovering show merely a small amplitude of resistance changes, indicating the successful construction of stable and continuous conductive networks (see fig. S11 for the activation curves of other samples with different concentrations of fluoroelastomer). Note also that the two-step activation process will not be a big obstacle for the scale-up production of conductive LM sheath-core microfibers since the seemingly cumbersome stretching process may be replaced by continuous cold drawing via adjusting the rotating velocities of fast and slow rollers (*45*). Moreover, even as the LM composite core has been fully activated with a percolated LM phase, no LM leakage was observed after sonicating a cut fiber in water for 2 hours (fig. S12), suggesting the high affinity of LM to the microporous fluoroelastomer matrix.

The relative change in resistance, $\Delta R/R_0$ [$=(R - R_0)/R_0$], is generally used to evaluate the conductance changes at specific strains. As presented in Fig. 2D, the $\Delta R/R_0$ changing curves of the prepared LM sheath-core microfibers are all below that of pure LM, which obeys the Pouillet's law, and remain in a very small variation range even as stretched to more than 300% strain (see real-time demonstration in movie S1). The quantified $\Delta R/R_0$ values at different strains of LM sheath-core microfibers with different concentrations of fluoroelastomer (denoted as $C_{\text{PVDF-HFP-TFE}}$) in the core were plotted in Fig. 2E for comparison. Apparently, the microfiber with $C_{\text{PVDF-HFP-TFE}}$ = 7 wt % presents the best performance of strain-insensitive conductance, with the resistance changes of 2.1, 4.1, 10.5, and 34.9% at the strains of 100, 200, 300, and 400%, respectively. This result was well reproduced by comparing the values of three batches of wet-spun microfibers using the same recipe (fig. S13), indicating the high reliability of our method. It is presumed that too much fluoroelastomer in the core may lead to the incomplete percolation of LM particles, and too less fluoroelastomer cannot sufficiently reshape the LM phase for enhanced conductivity with stretch (will be discussed in the latter part). We compared the electrical performance of the present LM sheath-core microfibers with the currently reported strain-insensitive and LM-based stretchable fiber conductors (*7*, *8*, *20*–*22*, *28*, *29*, *46*–*48*) on the basis of maximum strain, initial conductivity, and $\Delta R/R_0$ at 200% strain. As shown in Fig. 2F and table S1, while some references did not optimize for stable conductance, the LM sheath-core microfibers show comparatively excellent performance in terms of all the three evaluation parameters

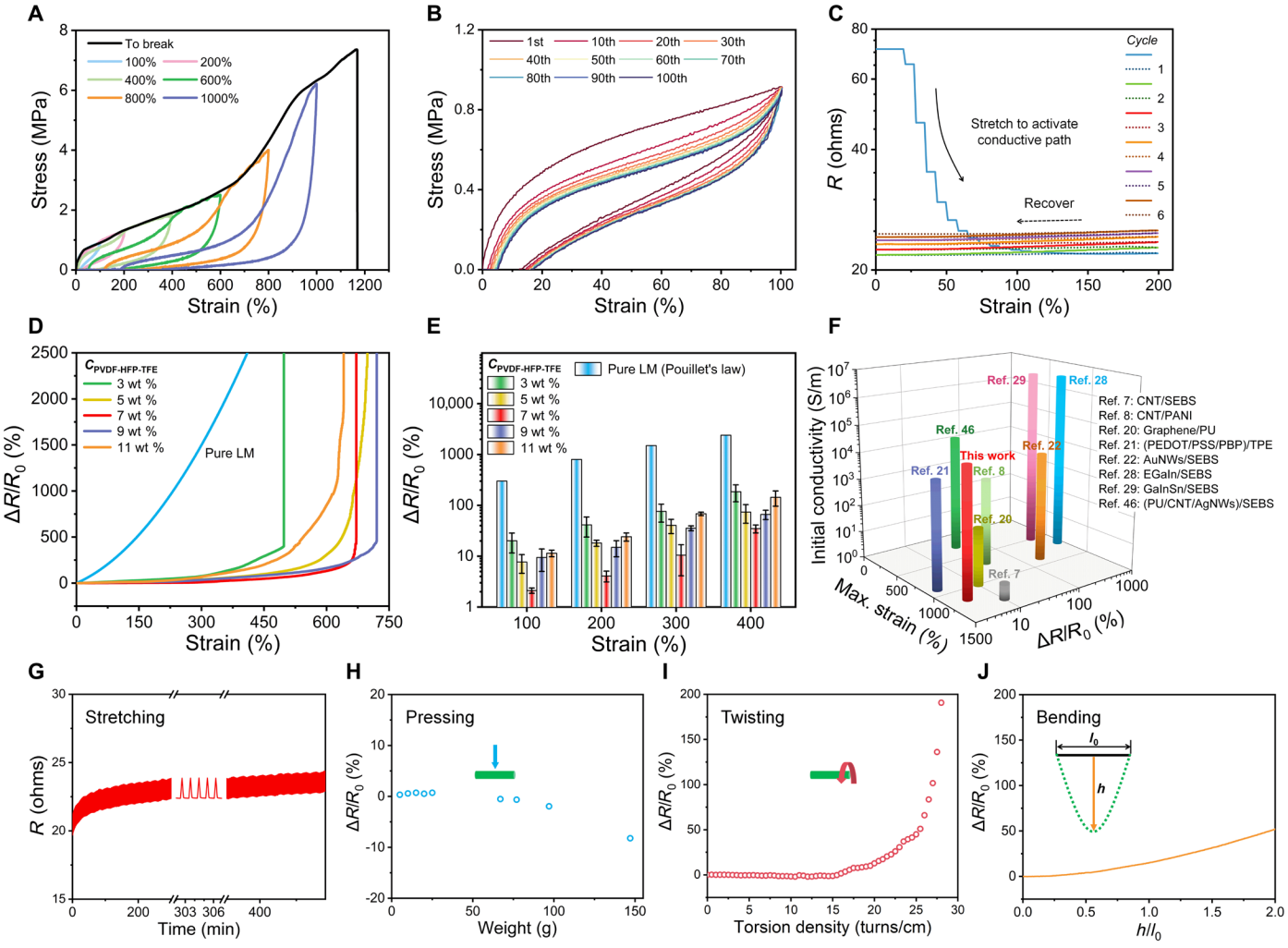

Fig. 2. Mechanical properties and strain-insensitive conductance of LM sheath-core microfibers. (**A**) Tensile stress-strain curves of LM sheath-core microfibers and the hysteresis loops measured at increasing strains (stretching rate: 20 mm/min). (**B**) Cyclic loading-unloading curves at a fixed strain of 100% for 100 cycles (stretching rate: 20 mm/min; waiting time: 10 min). (**C**) Resistance changes of the stretch-induced conductivity activation of microfiber after freezing treatment. (**D**) Strain-dependent resistance changing rate of LM sheath-core microfibers with six different fluoroelastomer loadings [$C_{PVDF\text{-}HFP\text{-}TFE}$ = 0 (pure LM), 3, 5, 7, 9, and 11 wt %]. (**E**) Histogram of resistance change rates at fixed strains of different microfibers. (**F**) Comparison of the maximum strain, initial conductivity, and resistance change rate at 200% strain of LM sheath-core microfiber with other reported strain-insensitive and LM-based stretchable fiber conductors. (**G**) Resistance changes of the LM sheath-core microfiber over 600 cycles between 0 and 100% strain. (**H** to **J**) Resistance changes of the microfiber upon pressing, twisting, and bending.

toward highly conductive, superelastic, and conductance-stable fiber conductors. To demonstrate the advantage of strain-insensitive conductance, the same LED was lit up through LM sheath-core microfiber and LM-filled silicone tube, respectively; stretching LM sheath-core microfiber to 400% strain led to almost unchanged brightness of LED, while stretching the LM-filled silicone tube to the same strain induced apparently diminished emitted light (fig. S14).

The excellent strain-insensitive conductance of the microfiber lead us to further study the stability and durability of electrical properties in the real application scenarios. As indicated in Fig. 2G, 600 cycles' stretching and recovering cause fully repeatable resistance changes in a very small amplitude, and the slight resistance baseline shift may be caused by the gradually optimized conductive path in the cycling process. In addition, the conductance of the sheath-core microfiber is also very stable during other forms of deformations such as pressing, twisting, and bending (Fig. 2, H to J, and movies S2 to S4). Upon pressing, when the mass of the load on the fiber reaches about 150 g, the instantaneous change in resistance does not exceed 10% (Fig. 2H). Even higher mass of load up to 3 kg may largely flatten the fiber but did not quickly destroy the conductive path (movie S2). Twisting is another common type of deformation for fibers, and the resistance of LM sheath-core microfiber only remarkably increases when the torsion density is above 15 turns/cm (Fig. 2I and movie S3). Bending is a kind of deformation comprising both stretching and pressing, and a high h/l_0 ratio of 2.0 (as denoted in Fig. 2J and movie S4) leads to only approximately 50% resistance change. All these results reveal that the high yet strain-insensitive conductance of LM sheath-core microfiber is not largely affected by the deformation type, conducive to its practical applications in smart fabrics and wearable electronics.

Mechanism discussion for strain-insensitive conductance

To elucidate the exact reason for the excellent strain-insensitive conductance behavior of LM sheath-core microfiber, we first investigated the interactions between fluoroelastomer and LM. LM has very high surface tension and is normally difficult to spread on solid surfaces. Nevertheless, as shown in Fig. 3A, we dropped an EGaIn LM droplet on the PVDF-HFP-TFE film, and then, stretching the film to 600% strain lead to the spontaneous deformation of the LM droplet with the increased contact area. The releasing process reveals a fully recoverable LM shape deformation, suggesting that LM should be able to reconciliate its surface to form a firm interface with fluoroelastomer (*49*). We attribute the self-regulated deformation of LM on fluoroelastomer to the strong dipole-dipole interactions between the Ga_2O_3 oxidation layer of LM and abundant polar C-F groups in PVDF-HFP-TFE, as illustrated in Fig. 3B (*50*). The presence of the surface oxidation layer on the used LM particles is clearly supported from the Ga 3d x-ray photoelectron spectroscopy (XPS) spectrum (Fig. 3C) (*51*, *52*). Further evidence for the dipolar interactions is provided by the infrared spectral comparison between pure PVDF-HFP-TFE and PVDF-HFP-TFE/LM composite (Fig. 3D), which shows an apparent peak shift of C-F stretching bands from 1149/1132 to 1214 cm^{-1}, suggesting remarkable changes of the chemical environment of C-F groups upon contact with LM particles. Although surface hydroxyl groups may also exist in the oxidation skin as indicated by O 1s XPS spectrum (fig. S15), the possibility of hydrogen bonding had been excluded, as the organic fluorine in fluoroelastomer is a poor hydrogen bond acceptor (*53*). As shown in fig. S16, if the oxide layer of EGaIn droplet was destroyed with hydrochloric acid, the droplet became more spherical, and stretching the film did not induce its deformation; further exposing the droplet in air for 24 hours to recover its oxide layer would recover the interfacial deformability again. All these results support the important role of the dipolar attraction between LM oxidation layer and fluoroelastomer in regulating LM deformation. In the case of the LM composite core of the studied microfiber, the high adhesion of LM particles with fluoroelastomer matrix would not only retain the hierarchical granular shape of percolated LM phase to avoid its free flow, as observed in fig. S12, but also promote the homogenous and reconciliatory deformation of LM for high conductance tolerance upon large deformations (*49*).

Nonetheless, merely strain-induced self-regulated deformation of LM particles is not sufficient to account for the observed

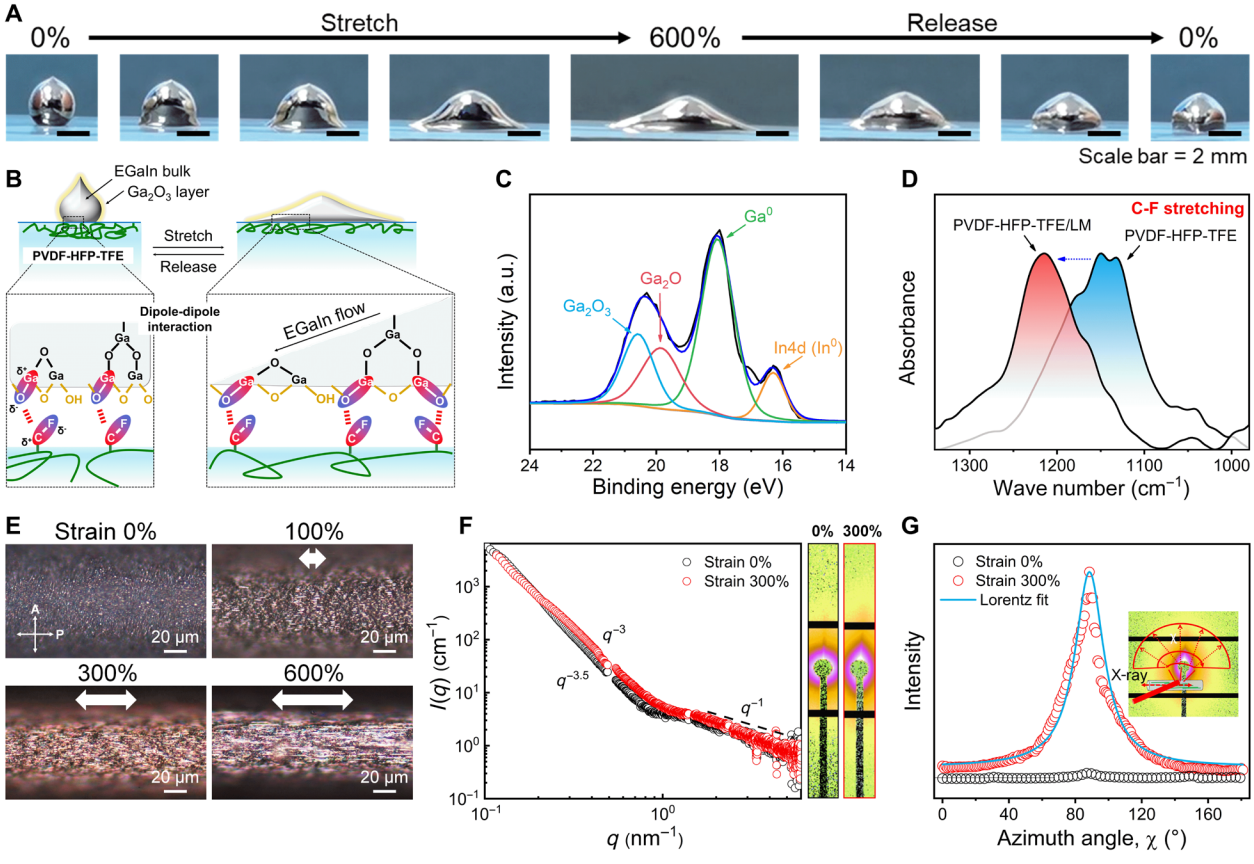

Fig. 3. Mechanism of the strain-insensitive conductance of LM sheath-core microfibers. (**A**) Photographs of EGaIn droplet surface reconciliation on PVDF-HFP-TFE film during stretching and releasing. (**B**) Schematic illustration of the surface creation and readjustment of EGaIn on the PVDF-HFP-TFE film through the dipole-dipole interactions between Ga_2O_3 layer and polar C-F groups. (**C**) Ga 3d XPS spectrum of LM particles. a.u., arbitrary units. (**D**) Attenuated total reflection–Fourier transform infrared (ATR-FTIR) spectra of PVDF-HFP-TFE and PVDF-HFP-TFE/LM composite ($C_{PVDF\text{-}HFP\text{-}TFE}$ = 7 wt %) in the C-F stretching region. (**E**) Polarizing micrographs of the LM sheath-core microfiber during stretching observed in the reflection mode. (**F**) 2D SAXS patterns and scattering intensity plots against *q* (the integration area is the selected rectangular area) of the microfiber at strains of 0 and 300%, respectively. (**G**) SAXS azimuth integration and corresponding Lorentz fitting curve. The inset picture is the 2D image of the fiber at 300% strain. Photo credit: Lijing Zheng, Donghua University.

counterintuitive low electromechanical coupling of LM sheath-core microfibers. We further used polarized optical microscope to track the elongation process of the fiber (Fig. 3E) and found that, at the initial undeformed state, the units of activated percolating LM network keep a spherical shape with sizes close to the as-prepared state. This means that adjacent LM particles or droplets connect to each other through very narrow channels presenting a typical "horseshoe-like" serpentine pattern, which may be maintained by the strong constraint of LM oxidation layer having good affinity with fluoroelastomer matrix. With stretch, larger LM microstructures started to appear, indicating the enhanced connection of LM particles, likely induced by the hydrostatic pressure of LM that flows into the neck to expand the channel. More clear evidence for the structural evolution of tortuously arranged LM particles in 0 to 50% strain has been presented in fig. S17. Meanwhile, as stretched, the original weakly oriented spherical LM particles gradually elongate into needle-like microstructures along the stretch direction, suggesting that more aligned conductive paths are formed.

Such microstructural changes of the fiber were further investigated by small-angle x-ray scattering (SAXS) method. The two-dimensional (2D) SAXS patterns, scattering intensity plots, and the azimuth integration with different strains are shown in Fig. 3 (F and G). The 2D SAXS results show elongated nucleus-like scattering patterns perpendicular to the fiber axis, and the corresponding azimuth plot exhibits a sharp distribution (full width at half maximum, $\approx 26^{o}$) at 300% strain, which means a very good preferential orientation. The presence of a turning point at the q value around 1 nm^{-1} suggests that there are at least two levels of structures in the fiber, corresponding to the microstructures less than 5 nm from fluoroelastomer chains and macroscopic structures larger than 100 nm from the percolated network, respectively. Moreover, the low q scattering curve of the microfiber at 0% strain shows a $q^{-3.5}$ scattering, which shifts to $q^{-3.0}$ at 300% strain, indicating the loss of fiber density after stretching as LM particles start to flow. All the above observations coincide with the recent computation results from Zolfaghari *et al.* (*54*) who explained the reduced electromechanical coupling of LM-embedded elastomers to mainly two principal contributions: One is the hydrostatic pressure–controlled opening of the narrow, neck-like connections among LM droplets, and the other one, probably the primary contribution, is the stretching out of the original highly tortuous serpentine conductive path, which does not prominently alter their length and average cross-sectional area to preserve the end-to-end conductance ($G = \sigma A/l$; where σ is the intrinsic conductivity of LM, A is the cross-sectional area, and l is the conductive length). A schematic mechanism for the strain-insensitive conductance of LM sheath-core microfiber is presented in fig. S18, which is reminiscent of the findings in other LM-embedded composites, LM-filled elastomer foams, and LM network on elastomer films (*36*, *38*, *40*, *49*).

Joule heating behaviors

We further explored the potential applications of LM sheath-core microfibers in smart fabrics. As the fiber is very fine with a rather small Young's modulus, knitting the fiber into fabrics does not lead to any big influence on the mechanical properties of the fabric (fig. S19). In terms of the high yet strain-insensitive conductance, the LM sheath-core microfibers may be used as an electrical heater via joule heating effect. To test the heating performance, we connected a DC voltage supplier to the two ends of the microfiber, and an infrared thermal camera was used to monitor temperature changes. As shown in Fig. 4A and movie S5, the temperature of the fiber increases uniformly and simultaneously with the applied DC voltage and reaches 71.9°C at the applied voltage of 1.2 V. The cyclic heating test (Fig. 4B) was performed by repeatedly applying a DC voltage of 0.8 V, showing repeatable temperature changes between 48.1°C and room temperature (24.2°C). The temperature switching is rather fast, with the heating time of 6.5 s and cooling time of 9 s (Fig. 4C). We also embedded the LM sheath-core microfiber in an elastic spandex fabric glove (Fig. 4D); as the fingers bend to stretch the fiber, owing to the strain-insensitive conductance, the joule heating effect is not largely influenced. In addition, microencapsulated thermochromic dyes (color degradation temperature, ≈30°C; see photos of the ink and SEM images in fig. S20) can also be blended into the sheath during wet-spinning to endow the fiber with electrothermochromic properties (*55*). As shown in Fig. 4E and movie S6, with the applied voltage of 0.45 V, the colored microfibers (green, red, and blue) rapidly turned to their intrinsic color of gray because of the thermally induced color changes of embedded dyes (temperature rose from 20° to 48.1°C). This process is fully reversible by switching the voltage on and off. Knitting the colored microfibers into a fabric with the letters "LMF" reproduced all the observed color changes (Fig. 4E). Moreover, at the constant applied voltage, pressing the microfiber would lastly increase the fiber's resistance and thus reduce joule heating power ($P = U^2/R$; U is the applied voltage), and the reversible color response was also observed (fig. S21). All these findings prove the microfiber's great potential in the intelligent display and adaptive camouflage of smart fabrics.

Self-powered sensing

LM sheath-core microfibers with consistently high conductance at large strains and very electronegative surface could act as ideal highly stretchable self-powered sensors based on the single-electrode-mode triboelectric mechanism (*31*, *56*, *57*). Figure 5A shows the working principle of self-powered sensing via LM sheath-core microfibers based on contact triboelectrification and electrostatic induction (*58*). For single-electrode-mode triboelectrics, the microfiber is connected to the ground through an external load. Once a moving object (most commonly used materials in our everyday life including human skin are triboelectrically positive) contacts with the fiber, electrification occurs at the interface and generates opposite charges at the surface of the two materials (Fig. 5A, i). When the two surfaces separate, the static charges on the surface of the sheath will induce the movement of electrons in the LM composite core to balance them (Fig. 5A, ii). When the moving object is approaching back to the microfiber, the whole process will be reversed with an electron flux with the opposite direction (Fig. 5A, iii and iv). Therefore, the movement of the target materials can be detected from either open-circuit voltage or the generated alternating current. Note that, among the common triboelectric materials, the chemical-resistant fluoroelastomer is reported to show the most negative triboelectric polarity, even higher than polytetrafluoroethylene (Fig. 5B) (*59*); meanwhile, the ultrasmall Young's modulus and ultrahigh stretchability of LM sheath-core microfibers make them quite suitable for imperceptible wearable sensing.

We thus monitored the induced voltage and current with LM sheath-core microfiber by repeatedly contacting with five different materials, viscose fabric, cotton fabric, ethylene-vinyl acetate copolymer, aluminum foil (Al), and silk fabric. As shown in Fig. 5C and fig. S22, highly reproducible electrical signals can be detected

depending on the materials with different triboelectric polarities, indicating that the LM sheath-core microfiber-based self-powered sensor is promising in identifying material types as per their electron affinity differences. Moreover, the voltage increased from 2.13 to 5.11 V and the current increased from 26.2 to 93 nA when the contact-separation frequency increased from 1 to 4 Hz (Fig. 5D and fig. S23), which may be ascribed to the enhanced flow rate of charges caused by the higher deformation rates of microfiber at higher frequencies (*60*). As the microfiber was stretched to higher strains, the fiber-based sensor still worked and an increased voltage and current were observed with increasing strain yet fully recovered when the fiber was released (Fig. 5E and fig. S24). This increment can be attributed to the increase of contacting area and the thickness decrease of the sheath during stretching benefitting for electrification (*58*, *61*). We further tested the self-powered sensing ability of LM sheath-core microfibers for monitoring real human activities. As shown in Fig. 5F and fig. S25, the fiber-embedded fabric glove was worn on a prosthetic hand, and bending the finger would induce the friction between the LM microfiber and polyurethane fibers in the glove, thus causing similar voltage and current generation. Bending the finger to increasing angles induced repeatable yet increasing amplitudes of voltage and current changes (movie S7). Moreover, adhering the fiber on human wrist lead to similar results based on the friction between human skin and the fiber (Fig. 5G and

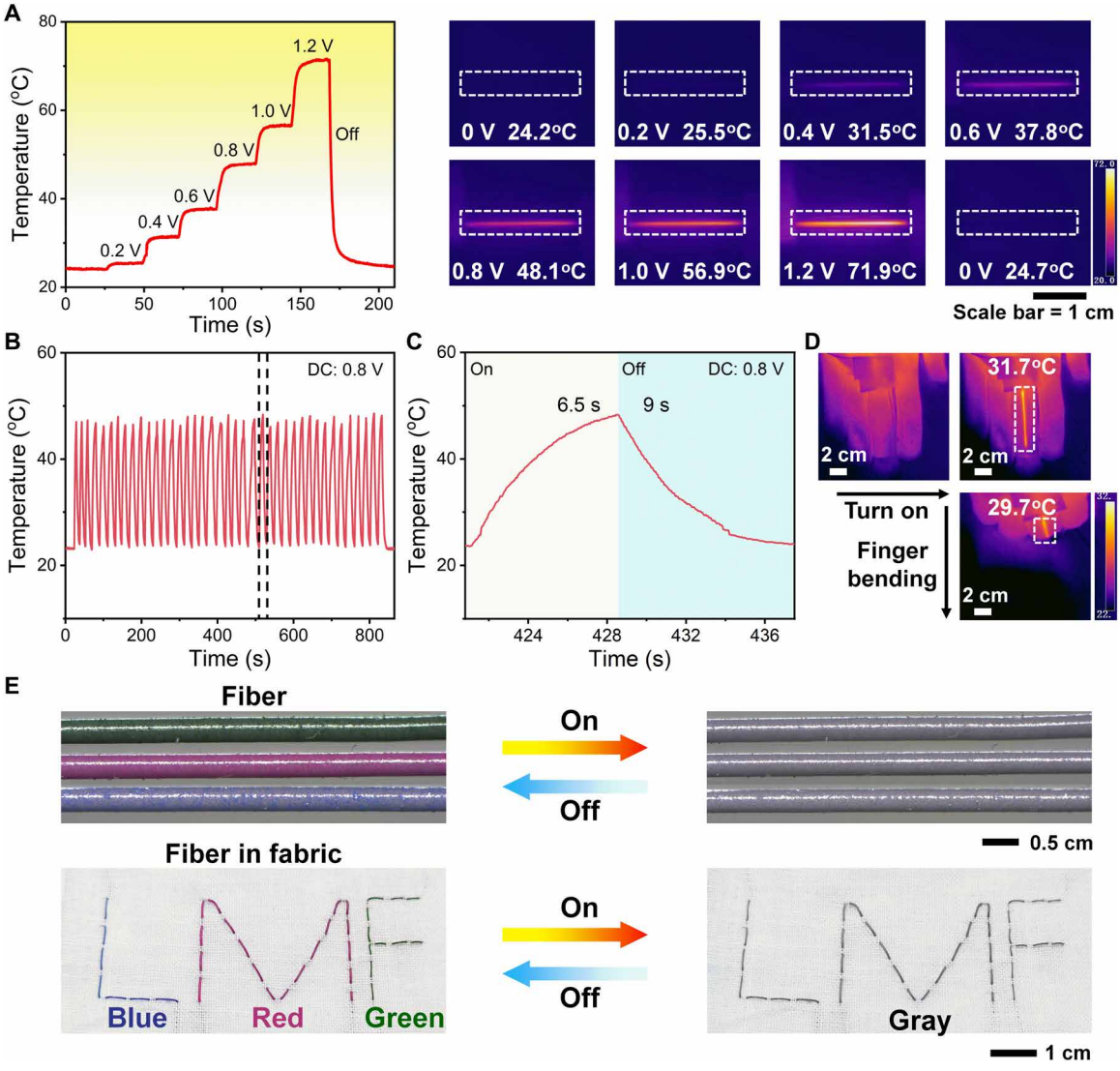

Fig. 4. Joule heating properties of LM sheath-core microfibers. (**A**) The stepwise temperature changing curve and corresponding infrared thermal images of the LM sheath-core microfiber with the applied voltage from 0 to 1.2 V. (**B**) Cyclic stability test of the joule heating performance of the microfiber by switching voltage between 0 and 0.8 V. (**C**) The enlarged image of the dashed area in (B) shows the temperature changes in one on-off cycle. (**D**) Infrared thermal images of the fiber embedded in an elastic fabric glove (applied voltage, 0.4 V) as the fingers bend. (**E**) Microscopic images of the electrothermochromic microfibers and photographs of the fibers embedded in a fabric by switching the voltage on and off. Photo credit: Lijing Zheng, Donghua University.

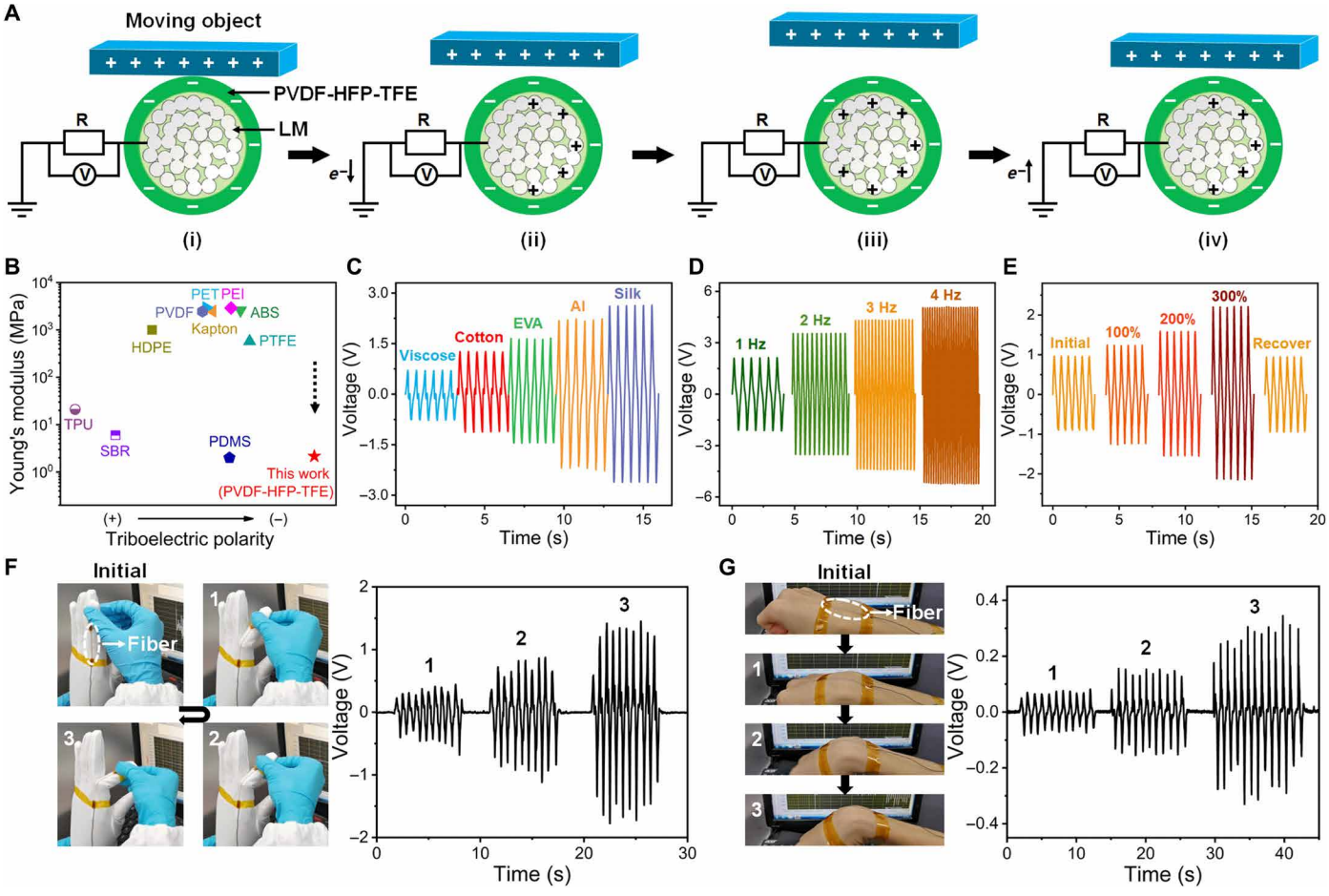

Fig. 5. Application of the LM sheath-core microfibers/fabrics in self-powered sensors. (**A**) Working mechanism of LM sheath-core microfiber-based self-powered sensor. (**B**) Comparison of the Young's moduli and relative triboelectric polarities of common triboelectric materials. (**C**) Voltage signals generated by contacting LM microfiber with five different triboelectric materials at the motion frequency of 2 Hz. The length of the fiber is 4 cm. (**D**) Voltage signals under different frequencies generated by contacting the fiber with silk. (**E**) Voltage signals under different strain levels of the fiber at the motion frequency of 2 Hz. The length of the fiber is 1 cm. (**F**) Photos and corresponding voltage signals by bending the fiber sensor–embedded spandex glove worn on a prosthetic hand. (**G**) Photos and corresponding voltage signals of the fiber sensor adhered to a human wrist. Photo credit: Lijing Zheng, Donghua University.

fig. S26), demonstrating the powerful sensing ability of LM sheath-core microfibers as self-powered wearable sensors.

DISCUSSION

Together, we herein reported a coaxial wet-spinning strategy based on LM particles and PVDF-HFP-TFE to fabricate highly conductive, intrinsically stretchable LM sheath-core microfibers with both high stretchability and strain-insensitive conductance. Superior to the strain-insensitive fiber conductors prepared by commonly used prestrain buckling and helical structure method, the wet-spun microfibers can be continuously fabricated and have ultrahigh conductivity and conductance stability after a freezing-plus-stretching activation process to sinter LM particles, and repeatable deformations including stretching, pressing, twisting, and bending do not cause the remarkable deterioration of their electrical performance. We attribute the strain-insensitive conductance of LM sheath-core microfibers to both the hydrostatic pressure–induced opening of LM particle connections and the straightening of the highly tortuous serpentine conductive paths of percolated LM network as confined by fluoroelastomer chains via dipolar interactions. Benefitting from the high conductivity, low Young's modulus, and very electronegative fluoroelastomer sheath, we further demonstrate the applications of the microfibers in both joule heating, electrothermochromism, and self-powered sensing, which may gain potential uses in both smart textiles and wearable sensors.

MATERIALS AND METHODS

Materials

EGaIn (Ga, 75.5%, and In, 24.5% by weight; melting point, ~15.7°C) was purchased from Wochang Co. Ltd. PVDF-HFP-TFE was purchased from Qingheng. The photoinitiator, Irgacure 184, was purchased from IGM Resins. PEGDA (average M_n = 250 g/mol) was purchased from Sigma-Aldrich. MEK was acquired from Sinopharm Chemical Reagent Co. Ltd., China. Benzotrifluoride was purchased from Aladdin Reagent (Shanghai). Microencapsulated thermochromic inks (green, red, and blue; color degradation temperature, ≈30°C;

solvent, cyclohexanone; concentration, 25 wt %; capsule size, 1 to 10 μm) were purchased from Magic Color Change Technology (Shenzhen). All the above reagents were used without further purification. DI water (18.2 megohms/cm) was used unless stated otherwise.

Preparation of spinning solutions

PVDF-HFP-TFE solution was prepared by dissolving PVDF-HFP-TFE in MEK at a concentration of 360 mg/ml. To prepare LM dispersions, LM was placed in a centrifuge tube containing MEK and probe-sonicated (power, ~300 W; Scientz, JY92-IIN) in an ice water bath for 30 min. For the inner spinning solution, PVDF-HFP-TFE solution was mixed with the LM dispersion to reach a final polymer concentration of 300 mg/ml. For the middle spinning solution, the mass ratio of PVDF-HFP-TFE:Irgacure 184:PEGDA is 100:2:4. DI water was used as both the outer spinning solution and coagulating bath.

Wet-spinning of LM sheath-core microfibers

All the spinning solutions were defoamed with a degassing machine before use and then injected via a custom-designed triaxial needle with the size of 22 gauge–13 gauge–10 gauge (corresponding to the inner, middle, and outer diameters of 400, 1950, and 3000 μm, respectively). As shown in fig. S1, the flow rates of the inner (2.0 ml/hour), middle (4.0 ml/hour), and outer (4.0 ml/hour) spinning solutions were controlled by syringe pumps. The cured LM sheath-core microfibers were collected via a winding collector at a rotation speed of 12 rpm (the diameter of the drum is 9 cm).

Cross-linking of PEGDA in the sheath of microfibers

To improve the elastic recovery of LM sheath-core microfibers, we introduced a second network into the sheath. To initiate the polymerization of the embedded PEGDA chains in the sheath, the dried as-spun microfibers were put under (365 nm, 40 W) for 10 min.

Fabrication of electrothermochromic LM sheath-core microfibers

To prepare electrothermochromic microfibers, thermochromic ink with specified color was added to the outer spinning solution with a final concentration of about 30 mg/ml, while other conditions remain unchanged.

SAXS measurements

SAXS experiments were performed at the Shanghai Synchrotron Radiation Facility beamline BL16B at an x-ray energy of 10.0 keV, which corresponds to a wavelength of $\lambda = 1.24$ Å. The sheath-core microfibers were measured perpendicular to the beam with a sample-detector distance of 1.9 m to cover the scattering vector $\mathbf{q}$ range from 0.03 to 1.5 nm^{-1} ($\mathbf{q}$ is the scattering vector; $\mathbf{q} = (4\pi/\lambda)\sin(\theta)$; 2θ is the scattering angle). The scattering patterns were obtained with a short exposure time (10 s), and the air background was subtracted. The SAXS pattern was azimuthally and radially averaged to obtain the intensity profile.

Self-powered sensing

For self-powered sensing, the fiber was put horizontally, and the dielectric material was adhered to a linear motor (LinMot, E1100) equipped in a Mark-10 dynamometer to provide periodic and programmed mechanical movements. The external load resistance was 100 megohms. The electrical signals of the LM sheath-core microfibers were recorded with an electrometer (Keithley 6514). The acquired data were recorded and analyzed in real time using a customized LabVIEW software program. The length of a single LM sheath-core microfiber for testing different friction materials and frequencies is 4 cm, and the length of the fiber for testing different strains is 1 cm (unless otherwise specified, the test tap strength of the fiber is 5 N). For testing different frequencies, the contact frequency between silk and the fiber was controlled by the linear motor. For testing different strains, we stretch the microfiber to a certain strain and then let silk touch the fiber at the motion frequency of 2 Hz.

SUPPLEMENTARY MATERIALS

Supplementary material for this article is available at http://advances.sciencemag.org/cgi/content/full/7/22/eabg4041/DC1

REFERENCES AND NOTES

1. D. C. Kim, H. J. Shim, W. Lee, J. H. Koo, D.-H. Kim, Material-based approaches for the fabrication of stretchable electronics. *Adv. Mater.* **32**, 1902743 (2020).
2. F. Hartmann, M. Baumgartner, M. Kaltenbrunner, Becoming sustainable, the new frontier in soft robotics. *Adv. Mater.* **32**, 2004413 (2020).
3. D. G. Mackanic, M. Kao, Z. Bao, Enabling deformable and stretchable batteries. *Adv. Energy Mater.* **10**, 2001424 (2020).
4. Y. J. Tan, H. Godaba, G. Chen, S. T. M. Tan, G. Wan, G. Li, P. M. Lee, Y. Cai, S. Li, R. F. Shepherd, J. S. Ho, B. C. K. Tee, A transparent, self-healing and high-κ dielectric for low-field-emission stretchable optoelectronics. *Nat. Mater.* **19**, 182–188 (2020).
5. B. Wang, A. Facchetti, Mechanically flexible conductors for stretchable and wearable e-skin and e-textile devices. *Adv. Mater.* **31**, 1901408 (2019).
6. J. Xiong, J. Chen, P. S. Lee, Functional fibers and fabrics for soft robotics, wearables, and human-robot interface. *Adv. Mater.* **32**, 2002640 (2020).
7. Z. F. Liu, S. Fang, F. A. Moura, J. N. Ding, N. Jiang, J. Di, M. Zhang, X. Lepró, D. S. Galvão, C. S. Haines, N. Y. Yuan, S. G. Yin, D. W. Lee, R. Wang, H. Y. Wang, W. Lv, C. Dong, R. C. Zhang, M. J. Chen, Q. Yin, Y. T. Chong, R. Zhang, X. Wang, M. D. Lima, R. Ovalle-Robles, D. Qian, H. Lu, R. H. Baughman, Hierarchically buckled sheath-core fibers for superelastic electronics, sensors, and muscles. *Science* **349**, 400–404 (2015).
8. Z. Zhang, J. Deng, X. Li, Z. Yang, S. He, X. Chen, G. Guan, J. Ren, H. Peng, Superelastic supercapacitors with high performances during stretching. *Adv. Mater.* **27**, 356–362 (2015).
9. Y.-Y. Lee, H.-Y. Kang, S. H. Gwon, G. M. Choi, S.-M. Lim, J.-Y. Sun, Y.-C. Joo, A strain-insensitive stretchable electronic conductor: PEDOT:PSS/acrylamide organogels. *Adv. Mater.* **28**, 1636–1643 (2016).
10. Z. Liu, D. Qi, G. Hu, H. Wang, Y. Jiang, G. Chen, Y. Luo, X. J. Loh, B. Liedberg, X. Chen, Surface strain redistribution on structured microfibers to enhance sensitivity of fiber-shaped stretchable strain sensors. *Adv. Mater.* **30**, 1704229 (2018).
11. J. Lee, S. Shin, S. Lee, J. Song, S. Kang, H. Han, S. Kim, S. Kim, J. Seo, D. Kim, T. Lee, Highly sensitive multifilament fiber strain sensors with ultrabroad sensing range for textile electronics. *ACS Nano* **12**, 4259–4268 (2018).
12. S. Seyedin, S. Uzun, A. Levitt, B. Anasori, G. Dion, Y. Gogotsi, J. M. Razal, MXene composite and coaxial fibers with high stretchability and conductivity for wearable strain sensing textiles. *Adv. Funct. Mater.* **30**, 1910504 (2020).
13. Y. Gao, F. Guo, P. Cao, J. Liu, D. Li, J. Wu, N. Wang, Y. Su, Y. Zhao, Winding-locked carbon nanotubes/polymer nanofibers helical yarn for ultrastretchable conductor and strain sensor. *ACS Nano* **14**, 3442–3450 (2020).
14. M. Ju, B. Wu, S. Sun, P. Wu, Redox-active iron-citrate complex regulated robust coating-free hydrogel microfiber net with high environmental tolerance and sensitivity. *Adv. Funct. Mater.* **30**, 1910387 (2020).
15. L. Shuai, Z. H. Guo, P. Zhang, J. Wan, X. Pu, Z. L. Wang, Stretchable, self-healing, conductive hydrogel fibers for strain sensing and triboelectric energy-harvesting smart textiles. *Nano Energy* **78**, 105389 (2020).
16. G. Yun, S.-Y. Tang, S. Sun, D. Yuan, Q. Zhao, L. Deng, S. Yan, H. Du, M. D. Dickey, W. Li, Liquid metal-filled magnetorheological elastomer with positive piezoconductivity. *Nat. Commun.* **10**, 1300 (2019).
17. C. Choi, J. M. Lee, S. H. Kim, S. J. Kim, J. Di, R. H. Baughman, Twistable and stretchable sandwich structured fiber for wearable sensors and supercapacitors. *Nano Lett.* **16**, 7677–7684 (2016).
18. H. Wang, Z. Liu, J. Ding, X. Lepró, S. Fang, N. Jiang, N. Yuan, R. Wang, Q. Yin, W. Lv, Z. Liu, M. Zhang, R. Ovalle-Robles, K. Inoue, S. Yin, R. H. Baughman, Downsized sheath-core conducting fibers for weavable superelastic wires, biosensors, supercapacitors, and strain sensors. *Adv. Mater.* **28**, 4998–5007 (2016).

19. B. Zhang, J. Lei, D. Qi, Z. Liu, Y. Wang, G. Xiao, J. Wu, W. Zhang, F. Huo, X. Chen, Stretchable conductive fibers based on a cracking control strategy for wearable electronics. *Adv. Funct. Mater.* **28**, 1801683 (2018).
20. F. Sun, M. Tian, X. Sun, T. Xu, X. Liu, S. Zhu, X. Zhang, L. Qu, Stretchable conductive fibers of ultrahigh tensile strain and stable conductance enabled by a worm-shaped graphene microlayer. *Nano Lett.* **19**, 6592–6599 (2019).
21. J. Zhou, G. Tian, G. Jin, Y. Xin, R. Tao, G. Lubineau, Buckled conductive polymer ribbons in elastomer channels as stretchable fiber conductor. *Adv. Funct. Mater.* **30**, 1907316 (2020).
22. Y. Zhao, D. Dong, S. Gong, L. Brassart, Y. Wang, T. An, W. Cheng, A moss-inspired electroless gold-coating strategy toward stretchable fiber conductors by dry spinning. *Adv. Electron. Mater.* **5**, 1800462 (2019).
23. J. Lee, D. W. Kim, S. Chun, J. H. Song, E. S. Yoo, J. K. Kim, C. Pang, Intrinsically strain-insensitive, hyperelastic temperature-sensing fiber with compressed micro-wrinkles for integrated textronics. *Adv. Mater. Technol.* **5**, 2000073 (2020).
24. J. Woo, H. Lee, C. Yi, J. Lee, C. Won, S. Oh, J. Jekal, C. Kwon, S. Lee, J. Song, B. Choi, K.-I. Jang, T. Lee, Ultrastretchable helical conductive fibers using percolated Ag nanoparticle networks encapsulated by elastic polymers with high durability in omnidirectional deformations for wearable electronics. *Adv. Funct. Mater.* **30**, 1910026 (2020).
25. S. Gong, W. Cheng, One-dimensional nanomaterials for soft electronics. *Adv. Electron. Mater.* **3**, 1600314 (2017).
26. J. Yan, Y. Lu, G. Chen, M. Yang, Z. Gu, Advances in liquid metals for biomedical applications. *Chem. Soc. Rev.* **47**, 2518–2533 (2018).
27. L. Gu, S. Poddar, Y. Lin, Z. Long, D. Zhang, Q. Zhang, L. Shu, X. Qiu, M. Kam, A. Javey, Z. Fan, A biomimetic eye with a hemispherical perovskite nanowire array retina. *Nature* **581**, 278–282 (2020).
28. S. Zhu, J.-H. So, R. Mays, S. Desai, W. R. Barnes, B. Pourdeyhimi, M. D. Dickey, Ultrastretchable fibers with metallic conductivity using a liquid metal alloy core. *Adv. Funct. Mater.* **23**, 2308–2314 (2013).
29. Y. Qu, T. Nguyen-Dang, A. G. Page, W. Yan, T. Das Gupta, G. M. Rotaru, R. M. Rossi, V. D. Favrod, N. Bartolomei, F. Sorin, Superelastic multimaterial electronic and photonic fibers and devices via thermal drawing. *Adv. Mater.* **30**, 1707251 (2018).
30. S. Park, N. Baugh, H. K. Shah, D. P. Parekh, I. D. Joshipura, M. D. Dickey, Ultrastretchable elastic shape memory fibers with electrical conductivity. *Adv. Sci.* **6**, 1901579 (2019).
31. C. Dong, A. Leber, T. Das Gupta, R. Chandran, M. Volpi, Y. Qu, T. Nguyen-Dang, N. Bartolomei, W. Yan, F. Sorin, High-efficiency super-elastic liquid metal based triboelectric fibers and textiles. *Nat. Commun.* **11**, 3537 (2020).
32. H. Guo, Y. Han, W. Zhao, J. Yang, L. Zhang, Universally autonomous self-healing elastomer with high stretchability. *Nat. Commun.* **11**, 2037 (2020).
33. G. Chen, H. Wang, R. Guo, M. Duan, Y. Zhang, J. Liu, Superelastic EGaIn composite fibers sustaining 500% tensile strain with superior electrical conductivity for wearable electronics. *ACS Appl. Mater. Interfaces* **12**, 6112–6118 (2020).
34. R. Guo, H. Wang, G. Chen, B. Yuan, Y. Zhang, J. Liu, Smart semiliquid metal fibers with designed mechanical properties for room temperature stimulus response and liquid welding. *Appl. Mater. Today* **20**, 100738 (2020).
35. Y.-h. Wu, R.-m. Zhen, H.-z. Liu, S.-q. Liu, Z.-f. Deng, P.-p. Wang, S. Chen, L. Liu, Liquid metal fiber composed of a tubular channel as a high-performance strain sensor. *J. Mater. Chem. C* **5**, 12483–12491 (2017).
36. C. J. Thrasher, Z. J. Farrell, N. J. Morris, C. L. Willey, C. E. Tabor, Mechanoresponsive polymerized liquid metal networks. *Adv. Mater.* **31**, 1903864 (2019).
37. G. Yun, S.-Y. Tang, Q. Zhao, Y. Zhang, H. Lu, D. Yuan, S. Sun, L. Deng, M. D. Dickey, W. Li, Liquid metal composites with anisotropic and unconventional piezoconductivity. *Matter* **3**, 824–841 (2020).
38. B. Yao, W. Hong, T. Chen, Z. Han, X. Xu, R. Hu, J. Hao, C. Li, H. Li, S. E. Perini, M. T. Lanagan, S. Zhang, Q. Wang, H. Wang, Highly stretchable polymer composite with strain-enhanced electromagnetic interference shielding effectiveness. *Adv. Mater.* **32**, 1907499 (2020).
39. S. Ebnesajjad, *Introduction to Fluoropolymers* (William Andrew, ed. 1, 2013).
40. F. Krisnadi, L. L. Nguyen, Ankit, J. Ma, M. R. Kulkarni, N. Mathews, M. D. Dickey, Directed assembly of liquid metal-elastomer conductors for stretchable and self-healing electronics. *Adv. Mater.* **32**, 2001642 (2020).
41. H. Wu, Y. Cao, H. Su, C. Wang, Tough gel electrolyte using double polymer network design for the safe, stable cycling of lithium metal anode. *Angew. Chem. Int. Ed.* **57**, 1361–1365 (2018).
42. X. Zhang, B. Wu, S. Sun, P. Wu, Hybrid materials from ultrahigh-inorganic-content mineral plastic hydrogels: arbitrarily shapeable, strong, and tough. *Adv. Funct. Mater.* **30**, 1910425 (2020).
43. H. Wang, Y. Yao, Z. He, W. Rao, L. Hu, S. Chen, J. Lin, J. Gao, P. Zhang, X. Sun, X. Wang, Y. Cui, Q. Wang, S. Dong, G. Chen, J. Liu, A highly stretchable liquid metal polymer as reversible transitional insulator and conductor. *Adv. Mater.* **31**, 1901337 (2019).
44. X. Sun, B. Cui, B. Yuan, X. Wang, L. Fan, D. Yu, Z. He, L. Sheng, J. Liu, J. Lu, Liquid metal microparticles phase change medicated mechanical destruction for enhanced tumor cryoablation and dual-mode imaging. *Adv. Funct. Mater.* **30**, 2003359 (2020).
45. X. Liao, M. Dulle, J. M. de Souza e Silva, R. B. Wehrspohn, S. Agarwal, S. Förster, H. Hou, P. Smith, A. Greiner, High strength in combination with high toughness in robust and sustainable polymeric materials. *Science* **366**, 1376–1379 (2019).
46. Y. Zhang, W. Zhang, G. Ye, Q. Tan, Y. Zhao, J. Qiu, S. Qi, X. Du, T. Chen, N. Liu, Core-sheath stretchable conductive fibers for safe underwater wearable electronics. *Adv. Mater. Technol.* **5**, 1900880 (2020).
47. Y. Zhao, Q. Zhai, D. Dong, T. An, S. Gong, Q. Shi, W. Cheng, Highly stretchable and strain-insensitive fiber-based wearable electrochemical biosensor to monitor glucose in the sweat. *Anal. Chem.* **91**, 6569–6576 (2019).
48. Y. Yu, J. Guo, B. Ma, D. Zhang, Y. Zhao, Liquid metal–integrated ultra-elastic conductive microfibers from microfluidics for wearable electronics. *Sci. Bull.* **65**, 1752–1759 (2020).
49. J.-E. Park, H. S. Kang, M. Koo, C. Park, Autonomous surface reconciliation of a liquid-metal conductor micropatterned on a deformable hydrogel. *Adv. Mater.* **32**, 2002178 (2020).
50. S. Lee, J.-S. Park, T. R. Lee, The wettability of fluoropolymer surfaces: Influence of surface dipoles. *Langmuir* **24**, 4817–4826 (2008).
51. S. Handschuh-Wang, L. Zhu, T. Gan, T. Wang, B. Wang, X. Zhou, Interfacing of surfaces with gallium-based liquid metals—Approaches for mitigation and augmentation of liquid metal adhesion on surfaces. *Appl. Mater. Today* **21**, 100868 (2020).
52. Y. Ding, M. Zeng, L. Fu, Surface chemistry of gallium-based liquid metals. *Matter* **3**, 1477–1506 (2020).
53. J. D. Dunitz, R. Taylor, Organic fluorine hardly ever accepts hydrogen bonds. *Chem. A Eur. J.* **3**, 89–98 (1997).
54. N. Zolfaghari, P. Khandagale, M. J. Ford, K. Dayal, C. Majidi, Network topologies dictate electromechanical coupling in liquid metal-elastomer composites. *Soft Matter* **16**, 8818–8825 (2020).
55. Y. Jin, Y. Lin, A. Kiani, I. D. Joshipura, M. Ge, M. D. Dickey, Materials tactile logic via innervated soft thermochromic elastomers. *Nat. Commun.* **10**, 4187 (2019).
56. Y. Yang, N. Sun, Z. Wen, P. Cheng, H. Zheng, H. Shao, Y. Xia, C. Chen, H. Lan, X. Xie, C. Zhou, J. Zhong, X. Sun, S.-T. Lee, Liquid-metal–based super-stretchable and structure-designable triboelectric nanogenerator for wearable electronics. *ACS Nano* **12**, 2027–2034 (2018).
57. W. Wang, A. Yu, X. Liu, Y. Liu, Y. Zhang, Y. Zhu, Y. Lei, M. Jia, J. Zhai, Z. L. Wang, Large-scale fabrication of robust textile triboelectric nanogenerators. *Nano Energy* **71**, 104605 (2020).
58. X. Pu, M. Liu, X. Chen, J. Sun, C. Du, Y. Zhang, J. Zhai, W. Hu, Z. L. Wang, Ultrastretchable, transparent triboelectric nanogenerator as electronic skin for biomechanical energy harvesting and tactile sensing. *Sci. Adv.* **3**, e1700015 (2017).
59. Z. L. Wang, A. C. Wang, On the origin of contact-electrification. *Mater. Today* **30**, 34–51 (2019).
60. J. Zhong, Q. Zhong, F. Fan, Y. Zhang, S. Wang, B. Hu, Z. L. Wang, J. Zhou, Finger typing driven triboelectric nanogenerator and its use for instantaneously lighting up LEDs. *Nano Energy* **2**, 491–497 (2013).
61. Y. Yang, J. Han, J. Huang, J. Sun, Z. L. Wang, S. Seo, Q. Sun, Stretchable energy-harvesting tactile interactive interface with liquid-metal-nanoparticle-based electrodes. *Adv. Funct. Mater.* **30**, 1909652 (2020).
62. E. B. Twum, E. F. McCord, D. F. Lyons, P. L. Rinaldi, Multidimensional ^{19}F NMR analyses of terpolymers from vinylidene fluoride (VDF)-hexafluoropropylene (HFP)-tetrafluoroethylene (TFE). *Macromolecules* **48**, 3563–3576 (2015).
63. M. Shafiei, F. Hoshyargar, N. Motta, A. P. O'Mullane, Utilizing p-type native oxide on liquid metal microdroplets for low temperature gas sensing. *Mater. Des.* **122**, 288–295 (2017).

Acknowledgments: We thank the staff from BL16B beamline at the Shanghai Synchrotron Radiation Facility for assistance during data collection. **Funding:** We gratefully acknowledge the financial support from the National Science Foundation of China (NSFC) (nos. 21991123, 51873035, 51733003, and 21604024) and the "Qimingxing Plan" (19QA1400200). **Author contributions:** S.S. and P.W. conceived the project. L.Z. carried out all the experiments. M.Z. and Z.L. contributed to the self-powered sensing measurements. B.W. analyzed the SAXS results, and all authors provided meaningful feedback for the project and manuscript. **Competing interests:** The authors declare that they have no competing interests. **Data and materials availability:** All data needed to evaluate the conclusions in the paper are present in the paper and/or the Supplementary Materials. Additional data related to this paper may be requested from the authors.

Submitted 4 January 2021
Accepted 14 April 2021
Published 28 May 2021
10.1126/sciadv.abg4041

Citation: L. Zheng, M. Zhu, B. Wu, Z. Li, S. Sun, P. Wu, Conductance-stable liquid metal sheath-core microfibers for stretchy smart fabrics and self-powered sensing. *Sci. Adv.* **7**, eabg4041 (2021).